CrossMark

ORIGINAL PAPER

Nanoseismic monitoring of gravity-induced slope instabilities for the risk management of an aqueduct infrastructure in Central Apennines (Italy)

M. Fiorucci[1] · R. Iannucci[1] · L. Lenti[2] · S. Martino[1] ·
A. Paciello[3] · A. Prestininzi[1] · S. Rivellino[1]

Abstract A monitoring system is operative in the Peschiera Springs slope (Central Apennines, Italy) to mitigate the landslide risk related to the hosted main drainage plant of Rome aqueducts by providing alert warning. Such a strategy allows to avoid out-of-service episodes so reducing extra-costs of water distribution management. The Peschiera Springs slope is involved in a rock mass creep characterized by an average steady strain rate of 1 mm year^{-1} and responsible for several landforms including sinkholes, subvertical scarps and trenches. Moreover, an average aquifer discharge of 19 m^3 s^{-1} causes an intense limestone dissolution concentrated in correspondence with release bands and discontinuities that dislodge the jointed rock mass. Since 2008, an accelerometric network has been operating within the slope; about 1300 microseismic local events were recorded up to now, distinguished in failures and collapses. A control index, based on frequency of occurrence and cumulative energy of the recorded microseismic events was defined to provide three levels of alert. In 2013, a temporary nanoseismic Seismic Navigation System (SNS) array was installed inside a tunnel of the drainage plant to integrate the pre-existent seismic monitoring system. This array allowed to record 37 microseismic events, which locations are in good agreement with the evolutionary geological model of the ongoing gravitational slope deformation. In 2014, a permanent nanoseismic SNS array was installed in the plant and allowed to record several sequences of underground collapses including more than 500 events. The nanoseismic monitoring system is allowing to: (1) increase the detection level of the monitoring system; (2) locate hypocentres of the events; and (3) detect precursors of the strongest events.

✉ S. Martino
salvatore.martino@uniroma1.it

1   Dipartimento di Scienze della Terra and Research Center for Geological Risks CERI, "Sapienza" Università di Roma, Piazzale Aldo Moro 5, 00185 Rome, Italy

2   Institut Français des Sciences et Technologies des Transports, de l'Aménagement et des Réseaux (IFSTTAR-Paris), 14-20 Boulevard Newton Cité Descartes, Champs sur Marne, 77447 Marne-la-Vallée Cedex 2, France

3   Agenzia Nazionale per le Nuove Tecnologie, l'Energia e lo Sviluppo Economico Sostenibile (ENEA), C.R. Casaccia, Via Anguillarese 301, 00123 Rome, Italy

1 Introduction

The recognition of pre-failure events by seismic monitoring of natural systems is an important target to mitigate the geological risks due to abrupt failures. Changes in stress conditions of rock masses due to impulsive or viscous deformations can cause rapid and violent failures able to widely affect slopes and generate landslides or hypogeous collapses (Evans et al. 2006). The pre-failure behaviour of rock masses represents a complex geomechanical topic because the stress and jointing conditions as well as the joint setting can strongly constrain pre-failure effects, such as fractures generation, opening or closing of joints and readjustment of the stress field.

Sequences of microseismic events can proceed from a transitional to a transgressive phase so indicating incoming rock mass failures (Szwedzicki 2003). In this regard, the microseismic approach can be considered an useful tool for mitigating the natural risk in early warning perspective. Failure precursors were already detected by use of acoustic as well as seismometric devices (Deparis et al. 2008; Amitrano et al. 2010; Got et al. 2010). On the other hand, hypogeous instabilities triggered by impulsive events were recorded during experiments of controlled explosions and caves collapse in mine areas (Phillips et al. 1997). The analysis of sequences of precursors and post-failure events (i.e. underground instabilities induced by impulsive triggers) can be considered a suitable approach for managing early preventive interventions, as monitoring phases of failure propagation provides information on changes involving the rock mass, but also on possible occurrence of more critical conditions (i.e. generalized collapse). With respect to the more traditional seismometric network, microaccelerometers allow detecting vibrations with zero down to negative magnitudes (Butler 2003); moreover, high sampling frequencies (i.e. higher than 300 Hz) allow to locate vibrational events that attenuate faster than earthquakes. The nanoseismic monitoring approach was recently proposed (Joswig 2008) by using a specific geometry array called Seismic Navigation System (SNS) and a specific NanoseismicSuite software (developed by the Institute of Geophysics of Stuttgart University) to lower the magnitude of the recorded vibrations down to $-3M_L$ and fill the gap between microseismic networks and passive seismic.

A SNS array consists of a central three-component station and three outer vertical-component stations installed with an aperture between 25 and 100 m. Several experiments (Wust-Bloch and Joswig 2006; Walter et al. 2012a, 2012b; Sick et al. 2014) demonstrated the reliability of the nanoseismic technique to detect, locate and follow the space–time distribution of vibrational events related to rock mass instabilities such as landslides and sinkholes. Nonetheless, this technique was never tested in a permanent setting as part of an integrated monitoring system, where it is coupled with more traditional microseismic devices and geotechnical stress–strain sensors, in the aim to manage natural risks.

In this regard, the here presented results refer to a first experiment of coupling a nanoseismic SNS array in a wider monitoring system projected to manage the natural risk of landslides affecting the drainage plant of Rome aqueduct hosted in the Peschiera Springs slope (Lenti et al. 2012, 2015). Such a monitoring system, managed by the ACEA-ATO2 S.p.A. Italian Company, was planned and controlled by the Research Centre for Geological Risk (CERI) of the Sapienza University of Rome in co-operation with the Italian National

Agency for New Technologies, Energy and Sustainable Economic Development (ENEA) and the French Institute for Sciences and Technology for Transport, Development and Networks (IFSTTAR-Paris). Since the hazardous natural processes are unavoidable in the Peschiera Spring karst system, the adopted warning strategy aims at avoiding out-of-service episodes so reducing extra-costs for the water distribution manager and consequently the risk magnitude.

2 Geological and geomorphological setting of the Peschiera Springs slope

The Peschiera Springs slope corresponds to the south-western flank of Mt. Nuria (Central Apennines, Italy) and is composed of Malm–Lower Cretaceous limestones (Ciotoli et al. 2001; Bigi and Costa Pisani 2002). The structural setting of the slope is monoclinic, with EW-trending and N-dipping (30°–40°) strata; many fault lines cross the slope with roughly NS and N35E trends (Fig. 1).

The slope hosts a major karst aquifer which represents the drainage system of the Nuria-Velino-western Fucino and western Marsica Mountains (total area: 1016 km^2), whose main springs are the Peschiera-Canetra ones (measured total discharge: roughly varying from 18 up to 21 m^3 s^{-1}, according to Boni et al. 1986, 1995).
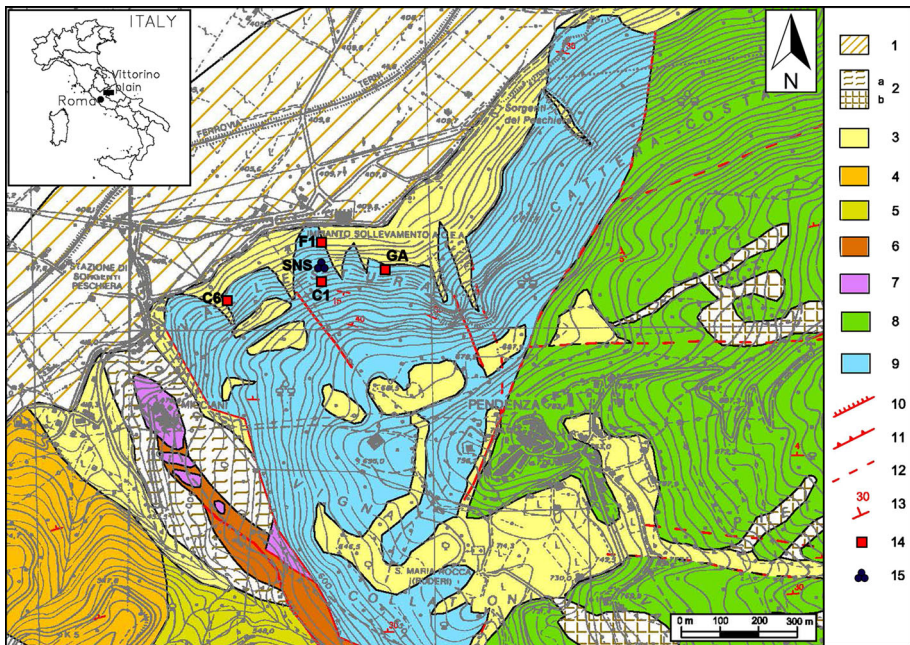

Fig. 1 Geological map of the Peschiera Springs slope: (*1*) recent alluvial deposits (Holocene); (*2*) Eluvio-colluvial deposits (Holocene): *a* silty clays and clayey silts, *b* reddish soils; (*3*) Slope debris (upper Pleistocene–Holocene); (*4*) Fosso Canalicchio Formation (upper Pliocene–lower Pleistocene); (*5*) Sandy-clayey Flysch (upper Miocene); (*6*) Marly limestone, marl and calcarenite (lower Miocene); (*7*) Scaglia formation (upper Cretaceous–lower Miocene); (*8*) *Salpingoporella* and Birdseyes limestone (lower Cretaceous); (*9*) Coral and Echinoids limestone (upper Jurassic); (*10*) Fault; (*11*) Thrust; (*12*) Supposed fault; (*13*) Attitude of beds; (*14*) Accelerometric station and (*15*) SNS array installed within the drainage plant

Geomorphological surveys performed on the slope as well as a digital high-resolution (2 m) elevation model (DEM), derived by a Light Detection And Ranging (LIDAR) radar remote survey, enabled to identify numerous landforms, e.g. scarps, trenches, sinkholes and tension cracks (Lenti et al. 2012), indicative of slow, intense and pervasive deformations, which affect the entire slope. These deformations correspond to different evolutionary stages ascribable to specific portions of the slope, as proved by already published result from a stress–strain monitoring system installed within the drainage plant (Martino et al. 2004; Maffei et al. 2005).

In particular, it is possible to recognize three sectors of the slope with ongoing gravity-induced processes: (I) a wide sector, including the southern portion of the slope and its top, with evidences of incipient and low deformations, i.e. in their early evolutionary stage; (II) a western sector, with evidences of mature and not yet advanced gravity-induced deformations, only concentrated close to the main trenches or scarps and (III) an eastern sector, with evidences of advanced gravity-induced slope deformations, characterized by pronounced landforms, such as scarps, trenches and sinkholes. Based on a frontal 3D view of the slope (Fig. 2), the rock mass spreading can be clearly observed in the western portion of the slope, where it is associated with multiple transverse trenches (i.e.continuous transverse scarps combined with longitudinal trenches) that generate a radial displacement field. In the eastern sector, a previous rock mass failure can be observed in the DEM; this failure generated two debris fans clearly visible at the bottom of the slope. The lateral 3D view of the DEM shows that the spreading process attributes a convex shape to the involved portion of the slope, while the scar area of the already occurred failure reveals a concave shape.

The geological-evolutionary model of the Peschiera Springs slope reflects a complex deep-seated gravitational deformation, which initiated a "sackung" phenomenon (Zischinsky 1969; Savage and Varnes 1987) continuously evolving from rock mass spreading (Hutchinson 1988) to rock block mass deformation (Martino et al. 2004).
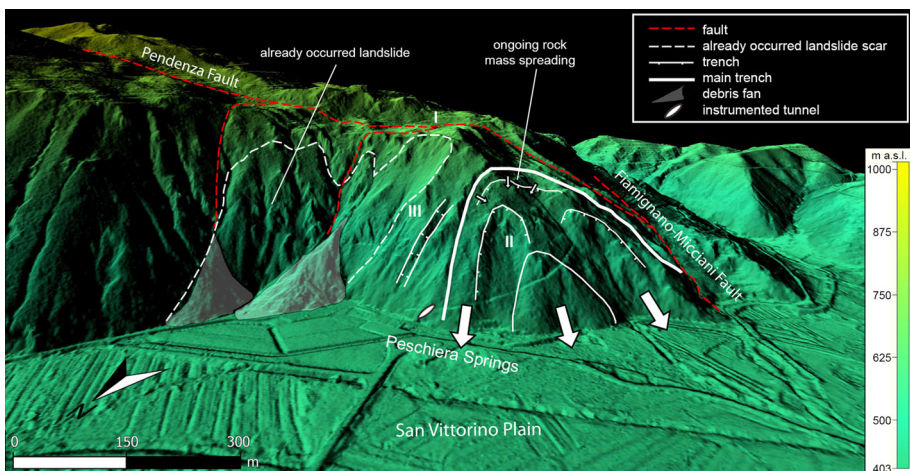

Fig. 2 3D view of the Peschiera Springs slope obtained from the 2-m-resolution DEM, illustrating the rock mass volume involved in the ongoing landslide processes and showing the main generated landforms. Slope sectors (I, II and III) at different evolutionary stages are also shown. The slope shapes reveal a convexity in the western sector, presently involved in the spreading process, and a concavity in the eastern sector was a general collapse already occurred. Arrows indicate the northward direction of the rock mass movement

The spreading is associated with the collapse of underground caves due to major karst dissolution within relieved rock mass portions, corresponding to subvertical belts (Maffei et al. 2005; Casini et al. 2006). These collapses result in a loss of volume at the surface with depressions and sinkholes. This process dislodged blocks, which increased the jointing of the rock mass. Furthermore, the collapse of underground caves may be triggered by external stresses, such as earthquakes (Maffei et al. 2005). Teleseismic events may interact with the dislodged blocks causing a temporary increase in the strain rate that induces displacements along joints up to 2 mm within 24 h (Lenti et al. 2015).

The ongoing deformational process that involves the Peschiera Springs slope also resulted from instrumental measurements performed through a geotechnical stress–strain monitoring system as well as by a traditional seismometric network installed inside the tunnels of the plant since almost 10 years (Lenti et al. 2012, 2015). An alarm system for managing the geological risk of the drainage plant was already tested (Lenti et al. 2012; Fiorucci et al. 2015), based on both frequency of occurrence and cumulative energy of the recorded events. In 2014, a SNS array devoted to record nanoseismic events was installed in a permanent configuration within the plant; the first outputs by this new monitoring system are here reported and discussed.

3 Seismic monitoring system

3.1 Accelerometric network and alarm system

Starting from 4 September 2008, four accelerometric stations (GA, C1, F1 and C6, see Fig. 1) were installed within the drainage plant of the Peschiera Springs in order to record both earthquakes and microseismic events originated within the slope and related to gravity-induced displacements. Each station is equipped with a three-component accelerometer KINEMETRICS Episensor (dynamic range 155 dB+, sensitivity 1.25 V g^{-1}; Fig. 3a), directly installed on bedrock, connected via cable to a 24-channel digital data logger KINEMETRICS Granite that is set to absolute local time through a GPS device and acquires with a 250 Hz sample frequency.

The trigger criteria of the data logger were set to record events characterized by different durations and large-band frequency content (Lenti et al. 2012). To automatically distinguish among different kinds of events, a specific script was implemented through Seismic Analysis Code (SAC) and Fortran codes on Unix platform. The software allows to classify the events on the basis of their physical properties, such as time durations, Fast Fourier Transform (FFT), amplitude Arias Intensity (AI) and Peak Ground Accelerations (PGA), and to distinguish among earthquakes and different microseismic events originated within the slope. In particular, microseismic events are distinguished in: (1) failures related to rock mass fracturing, with a duration from 1 to few seconds, and (2) collapses, with a duration less than 1 s and a typical waveform of impact (Walter et al. 2012b). The accelerometric network also records near-field and regional earthquakes as well as teleseismic events (Lenti et al. 2015).

The records obtained by the accelerometric network resulted to be a useful tool for managing the natural risk due to underground microseismic events at the Peschiera Springs drainage plant. For this purpose, the frequency of events (P) as well as the cumulative Arias Intensity (AI) of underground failures and collapses are plotted as a function of time.

To provide an alarm system for managing the geological risk of the plant, a frequency index [FI(P, t)] was defined as sum of two frequency indexes: the first referred to earthquakes
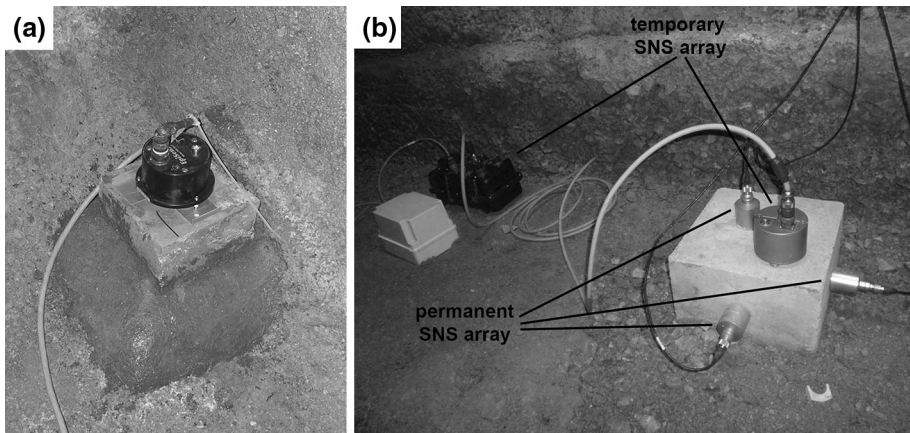
Fig. 3 Seismic monitoring system: **a** 3-component KINEMETRICS Episensor installed on rock at the C1 station of the accelerometric network; **b** 3-component Lennartz LE-3Dlite MkII seismometer and Reftek 130-01 data logger installed at the central station of the temporary SNS nanoseismic array, 1-component Brüel & Kjær type 8340 accelerometers installed at the central station of the permanent SNS nanoseismic array

[FI_er(P, t)] and another referred to microseismic events [FI_me(P, t)]. Moreover, the rate of the cumulative AI of the recorded microseismic events is used to define an energy index [EI(P, t)]. A final control index [CI(P, t)] was defined as a function of the sum of frequency and energy indexes [FI(P, t) + EI(P, t)]. This last index, daily computed for each station of the network, enables the association of each specific sector of the plant (represented by the corresponding accelerometric station) with three possible levels of alarm: the "ordinary" level (OL) if [CI(P, t) = 1]; the "alert" level (AL) if [CI(P, t) = 2]; and the "emergency" level (EL) if [CI(P, t) = 3]. To take into account particularly energetic events (collapses or failures), an alert threshold was fixed at a PGA value of 10^{-3} g, corresponding to the value that produced visible damages into the drainage plant (Lenti et al. 2012).

Until September 2015, the accelerometric network recorded 2311 events, including 1031 earthquakes and 1280 microseismic events (i.e. failures and collapses). Since January 2014, a relevant increase in the frequency of microseismic events, mainly due to collapses, was observed respect to the previous 7 years. From January 2014 to September 2015, the accelerometric network recorded 689 collapses, grouped in 46 crises, characterized by more than 3 events concentrated in few hours. As it results from the synoptic plot of Fig. 4a, the time distribution of the recorded crises could have been influenced by discharge variation, that affects the stress field within the karstified rock mass. The cumulative number of the recorded collapses shows a significant change in rate in correspondence with the maximum daily total discharge recorded (Fig. 4a); consequently, in these specific periods (September 2011, June–July 2014 and June–July 2015) the control index CI achieves the "emergency" level (Fig. 4b).

3.2 Nanoseismic array

During 2013, an experimental SNS nanoseismometric array was tested within the slope in abandoned drainage tunnels (see Fig. 1). The SNS records were managed by the NanoseismicSuite software (Joswig 2008; Sick et al. 2014) that includes two main tools: SonoView and HypoLine. SonoView allows to perform a data screening by the
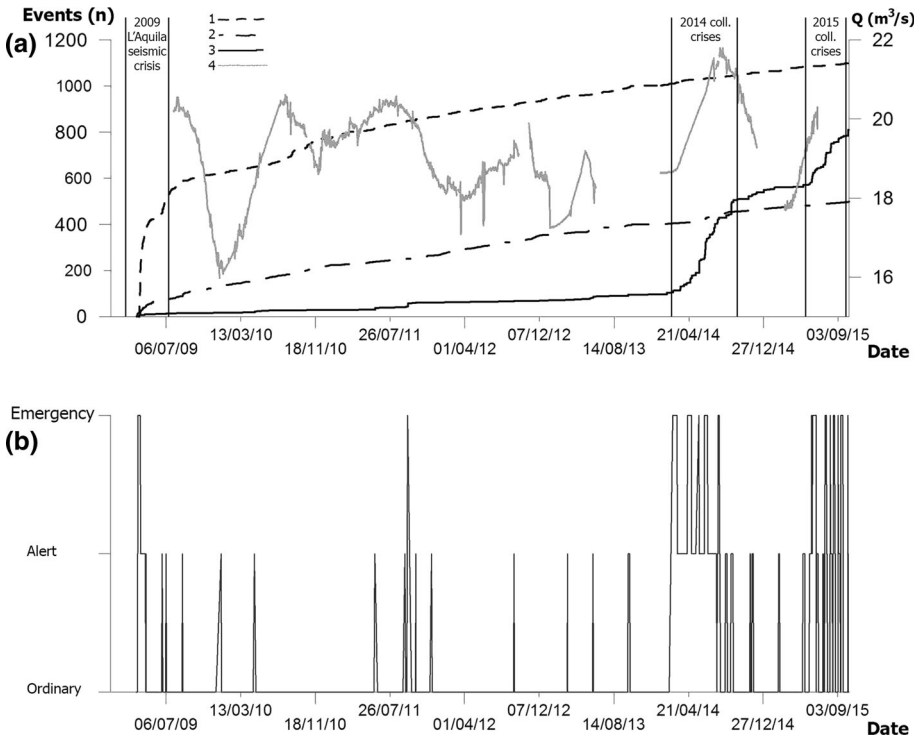
Fig. 4 a Cumulative numbers of (*1*) earthquakes, (*2*) failures and (*3*) collapses recorded by the accelerometric network; (*4*) the daily total discharge (data are not available where *line* is interrupted) is also shown; **b** variation of the alarm level at C1 station during the whole monitoring period (2008–2015) corresponding to the control index CI (*1*—ordinary; *2*—alert; *3*—emergency)

"supersonogram" operator, i.e. a specific spectrogram with noise adaptation, muting and pre-whitening function and a special colour palette that facilitates visual detection of seismic events. A main advantage of the sonograms is that they highlight event-related signals from stationary background noise (Joswig 1995). Stationary noise unrelated to the signal is filtered, allowing for a reliable detection even under challenging noise conditions. On the other hand, the localization of the events is carried out by HypoLine (Joswig 2008): this tool, based on a seismological approach, designs several shapes (i.e. 4 circles, 6 hyperbole, 2 beams) for locating the event source after a manual picking on the signal time-histories. This allows to assess hypocentre location as well as local magnitude M_L of the detected microseismic events.

Five measurement campaigns, with a duration ranging from 1 to 5 weeks, were carried out. Each station was equipped with one LE-3Dlite MkII seismometer (1 Hz period) by Lennartz Electronic GmbH and one REFTEK 130-01 data logger at 24 bit for channel (Fig. 3b) that acquired in continuous mode with a sampling frequency of 500 Hz.

Since the array was installed into the slope, each detected event was located by assuming two different velocity models (Fig. 5): one for the half-space below the array location level, the other for the upper half-space. The former was modelled as a homogeneous saturated half-space having V_P 2.7 km s^{-1} and V_S 1.5 km s^{-1}; the latter was characterized by two layers: the first layer (about 200 m thick and having V_P 2.7 km s^{-1} and V_S 1.8 km s^{-1}) represents a non-saturated rock mass, the second one is an infinite air
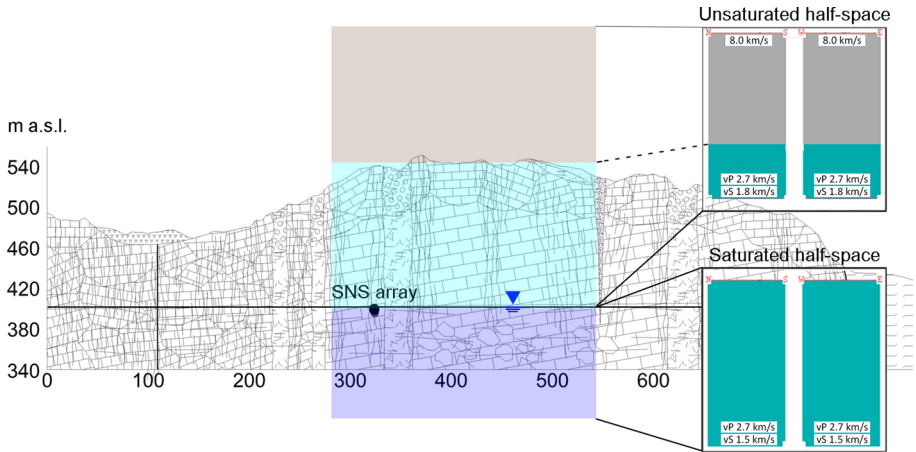
Fig. 5 Underground half-space models considered in the HypoLine software to locate the recorded microseismic events

half-space. The *P*-waves velocity values were attributed on the basis of geophysical investigations performed on the slope and within the drainage plant by ACEA S.p.A.

A physical characterization of the recorded signals was also carried out by a specifically implemented SAC (Seismic Analysis Code) script to uniform the different records (accelerometric and velocimetric) and to compute for each event the Peak Ground Acceleration (PGA) and Arias Intensity (AI) values according the following procedure:

- derivative of the velocity record to obtain the accelerometric record reducing the instrumental drift;
- filtering of the accelerometric signal considering the instrumental response;
- compute of the PGA as absolute maximum value of the time-history for vertical and horizontal components;
- compute of the AI for each component as: $\mathrm{AI} = \frac{\pi}{2g} \int_0^T a^2(t)\mathrm{d}t$.

The different microseismic events were distinguished by time duration and frequency content as well as by the considered physical parameters.

Based on the results obtained during the five measurement campaigns, a permanent SNS array was installed in 2014 to replace the temporal one. The permanent SNS array is equipped with 6 Brüel & Kjær type 8340 accelerometric sensors (Fig. 3b), having high sensitivity ($10\ \mathrm{V}\ \mathrm{g}^{-1}$) and flat response in acceleration in the frequency range 0.1–1500 Hz, coupled with a 3-modules HBM QuantumX data logger at 24 bit for channel that acquires in continuous mode at a 600 Hz sampling frequency.

4 Results of the nanoseismic array

4.1 Event characterization

During the five measurement campaigns of 2013, 37 microseismic events were detected. It was possible to distinguish the microseismic events (collapses and failures) from

earthquakes and teleseismic events as they differ in terms of time duration, amplitude, frequency content, magnitude and supersonogram pattern.

More in particular, using the "memory image" concept as a detection tool (Joswig 1990), the supersonogram allows to visualize that collapse events typically produce a sudden increase in intensity at certain frequencies, thus revealing their paroxysmal and impulsive nature; spikes are caused by the impacts of falling rock materials. Collapses typically enlighten the upper part of the supersonogram (Fig. 6), in a band ranging from about 30 up to 190 Hz with broadband spikes, as they are characterized by a higher frequency content respect to failures. More in particular, the 19 collapses detected during the experimental campaigns show maximum amplitudes (measured peak to peak) ranging from 300 up to 1500 nm s^{-1}. Their time duration can vary from less than 1 s to about 2 s. The time duration increases up to 3 or 4 s as in case of collapses of higher intensity or of multiple consecutive events. The computed M_L values vary from -3.4 up to -1.5.

The recorded collapses resulted mainly concentrated in two periods of the year (Fig. 7): 11 events were recorded in June 2013 within 25 days, and 7 events were recorded in September–October 2013 within 30 days. Due to a temporary out of order of the SNS array, further 6 collapses were recorded by the accelerometric network only and therefore it was not possible to characterize them.

As it resulted from the analysis of physical properties carried out by the customized SAC script (cfr. 3.2), the recorded collapses are characterized by PGA_h values (average between the two horizontal components) ranging from 10^{-5} up to 10^{-3} m s^{-2} with an average value of 10^{-3} m s^{-2} and AI_h values (average between the two horizontal components) ranging from 10^{-10} up to 10^{-7} m s^{-1} with an average value of 10^{-8} m s^{-1}.
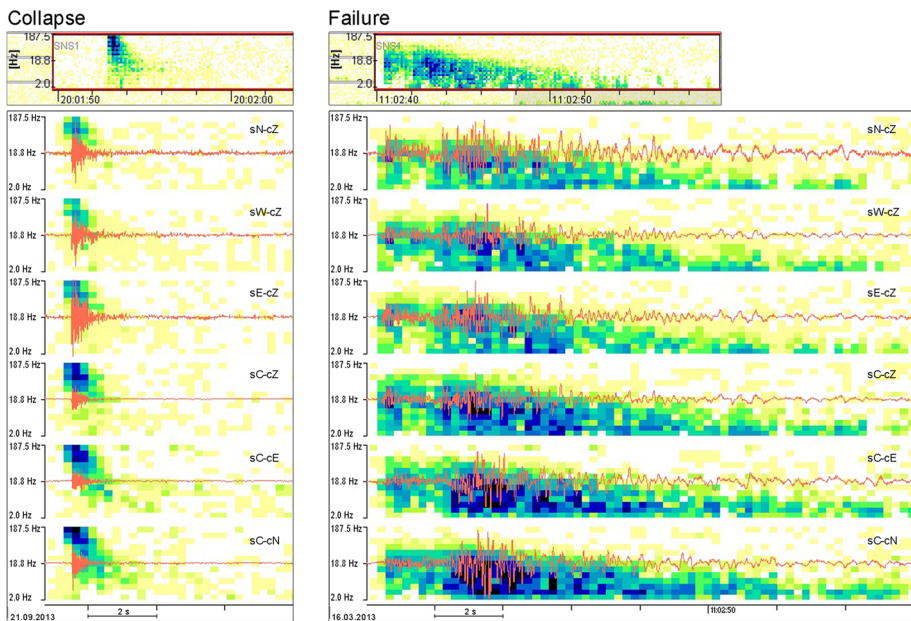

Fig. 6 Supersonogram (*top*), sonograms and over-layered waveforms (*bottom*) of the two typologies of events recorded in the Peschiera Springs slope by the SNS array: underground collapse event occurred on 21/09/2013 (*left*) and underground failure event occurred on 16/03/2013 (*right*). The upper three traces belong to the three outer vertical-component stations, the lower three traces belong to the central 3-component station
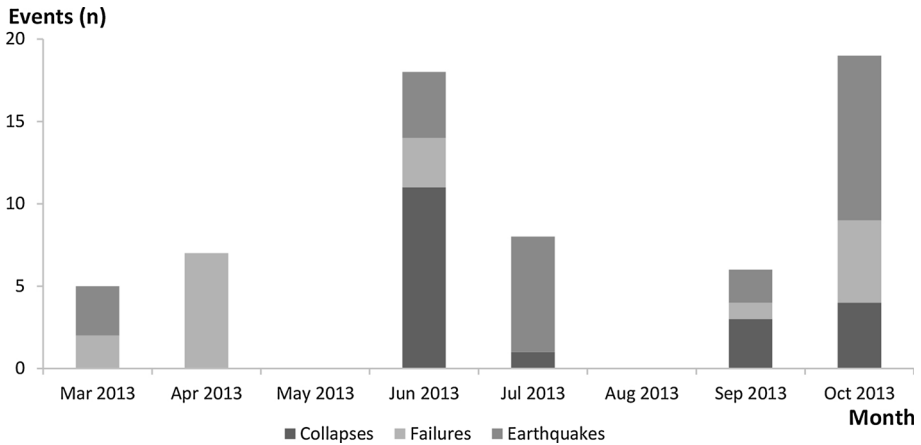
Events (n)

Fig. 7 Frequency histogram of microseismic events (collapses and failures) and earthquakes recorded by the SNS array during the five measurement campaign of 2013

During the five measurement campaigns, 18 microseismic events related to failures were also recorded. The analysis of the supersonograms allows to deduce a typical enlightening of the intermediate and low super-pixel (Fig. 6), i.e. in a range from about 5 up to 120 Hz with a low-frequency content in the event coda. These events show maximum amplitudes of 200–500 nm s^{-1}. Their time duration vary from 4 up to 7 s even if it can increases up to 15 s in case of higher magnitude events. The computed M_L values range from -1.9 up to -1.1.

As it regards the physical properties of the recorded failures, the PGA$_h$ values range from 10^{-5} up to 10^{-3} m s^{-2} with an average value of 10^{-4} m s^{-2}, and the AI$_h$ values range from 10^{-10} up to 10^{-8} m s^{-1} with an average value of 10^{-9} m s^{-1}. It is worth noticing that the microseismic events due to failures reveal AI$_v$ values (only related to the vertical component) at least one order of magnitude higher than the ones related to collapses.

Local and regional earthquakes as well as teleseismic events were also recognized and distinguished based on frequency contents, durations and physical features. Earthquakes and teleseismic events show comparable physical values wherever recorded in the plant as no attenuation occurs within the slope for these events; on the contrary, as it regards the microseismic events, the recorded PGA values are attenuated more than 40 % within the slope.

4.2 Collapse and failure hypocentre location

The epicentral distribution of the recorded events shows that most of them are located in the eastern sector of the Peschiera Springs slope (Fig. 8). By analysing the epicentral location in comparison with the observed landforms, it was observed that almost all the recorded collapses are focused along trenches and subvertical scarps and are concentrated in a sector of the slope where huge collapses already occurred, as in the case of the 1997 collapse occurred during the Umbria–Marche seismic sequence and documented by Maffei et al. (2005). It is worth noticing that such a distribution mainly corresponds to the sector of the slope where the maximum lowering of the groundwater table was induced by the drainage tunnels (Maffei et al. 2005). On the other hand, the recorded failures are mainly concentrated in the scar area that is located in the eastern portion of the slope (Figs. 8, 9), originated by the general failure of the slope occurred in pre-historical age (Martino et al. 2004).
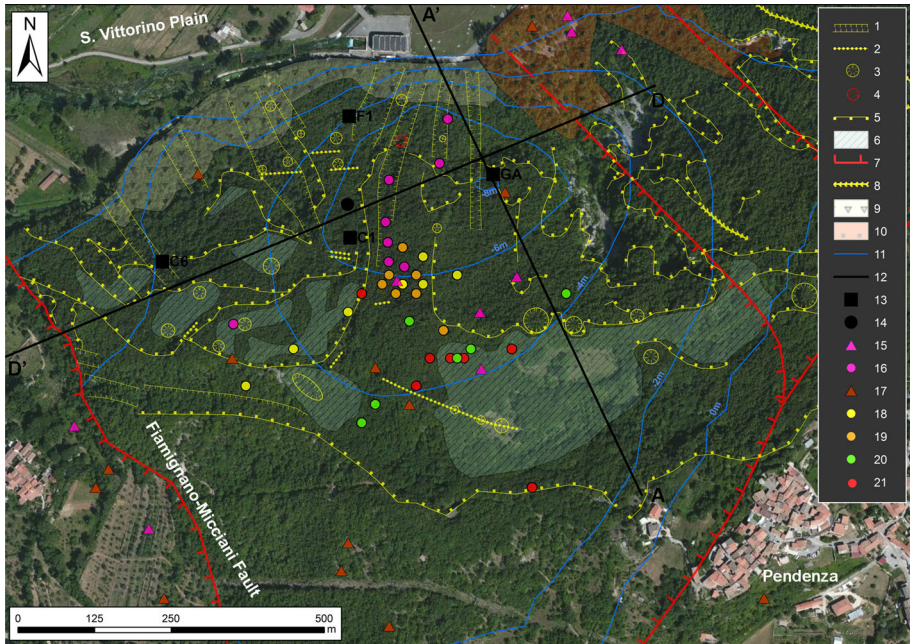
Fig. 8 Satellite view of the Peschiera Springs slope showing the main geomorphological features and epicentral distribution of the located microseismic events: (*1*) Trench; (*2*) Tension crack; (*3*) Sinkhole; (*4*) 1997 collapse of sinkhole; (*5*) Scarp; (*6*) Karstified flat; (*7*) Fault; (*8*) Gully; (*9*) Slope debris; (*10*) Debris fan deposit; (*11*) Groundwater level lowering due to the drainage plant; (*12*) Trace of the geological cross sections (see Fig. 9); (*13*) Accelerometric station and (*14*) SNS array position inside the drainage plant (derived from Maffei et al. 2005); (*15*) Failures and (*16*) collapses recorded by the experimental SNS array in 2013; (*17*) Failures recorded by the permanent SNS array in 2015; Collapses recorded by the permanent SNS array in 2015, during the (*18*) CC041, (*19*) CC046, (*20*) CC047 and (*21*) CC048 crises (see Table 1 for more details)

The obtained epicentral location of the recorded events is in very good agreement with the spatial distribution of the main morphological landforms associated with the ongoing rock mass deformation that involves the Peschiera Springs slope. Moreover, as it results from the hypocentre distribution, the underground instabilities are mainly located below the groundwater level and within an active volume which is about 150 m depth; this result is in very good agreement with the tension–dissolution model proposed through physical-analogue and numerical modelling (Maffei et al. 2005; Casini et al. 2006).

According to Walter et al. (2012b), the accuracy of hypocentre localization can be fixed to about 10 % of the epicentral distance. Therefore, since the hypocentral uncertainty depends to the array-epicentre distance, for the events originated within the slope it is varying from 5 up to 25 m for the furthest events.

5 Improvements in the seismic monitoring system by the permanent SNS array

The SNS nanoseismic array results to be a reliable tool for improving the detection of underground instabilities as it is contributing to identify sequences of very low-energy microseismic events that cannot be recorded by the traditional accelerometric network. The
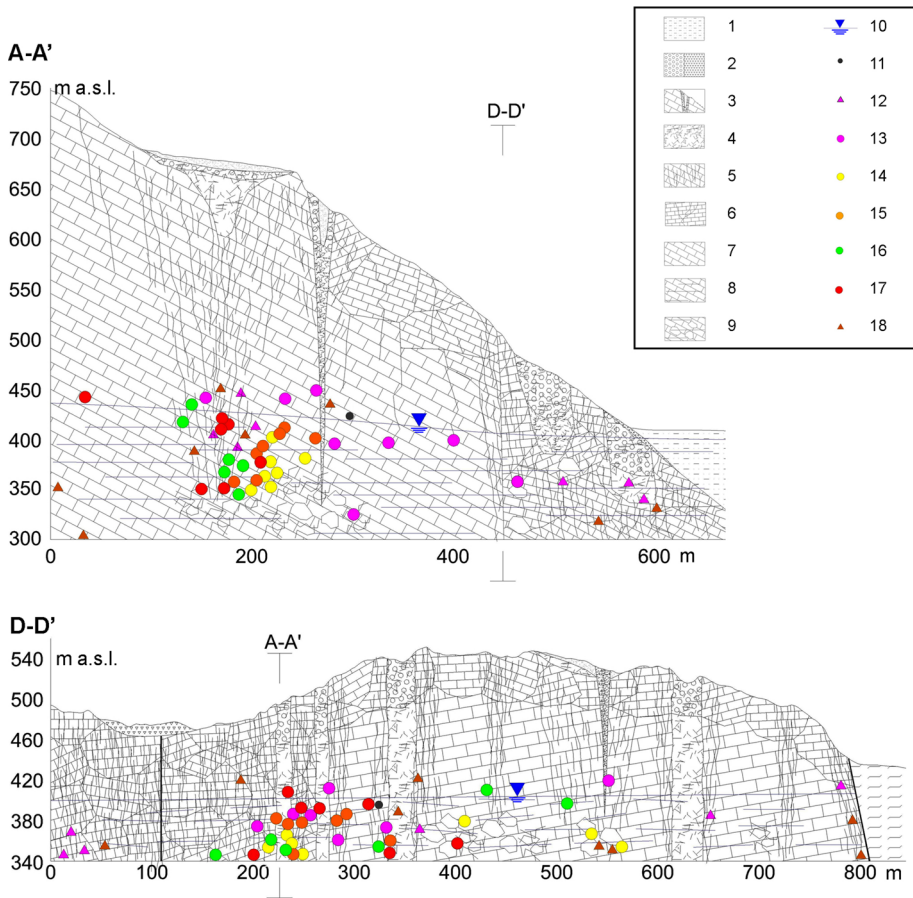
Fig. 9 Geological cross sections along traces A–A′ and D–D′ (see Fig. 8) of the Peschiera Springs slope showing the hypocentral distribution of the microseismic events recorded by the SNS array: (*1*) alluvial deposits of the San Vittorino plain; (*2*) trench and slope debris; (*3*) sinkhole; (*4*) intensely jointed rock mass; (*5*) concentration of failures in the rock mass; (*6*) dislodged rock mass; (*7*) rock mass located above the water table; (*8*) rock mass located in the rock aquifer; (*9*) underground caves in the karts aquifer; (*10*) groundwater level; (*11*) SNS array; (*12*) failures and (*13*) collapses recorded by the experimental SNS array in 2013; (*14*) failures recorded by the permanent SNS array in 2015; collapses recorded by the permanent SNS array in 2015, during the (*15*) CC041, (*16*) CC046, (*17*) CC047 and (*18*) CC048 crises (see Table 1 for more details)

total number of collapses recorded by the permanent SNS during the 14 collapse crises observed in 2015 (Fig. 10) is up to 8 times higher respect to the number of collapses recorded by the accelerometric network in the same period, as shown in Table 1 by the values of the detection ratio (ratio between the number of events detected by SNS array and the number of events detected by the accelerometric network). Figure 11 shows the supersonogram trace from 14:18 to 15:00 UTC hour on 25 July 2015; during this time, 37 events are detectable but only 2 collapses triggered by the accelerometric network as well.
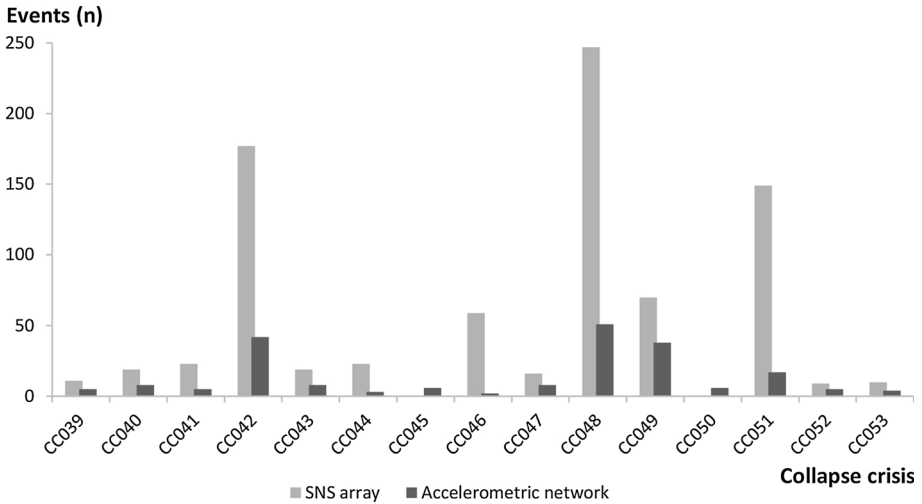
Events (n)

Fig. 10 Frequency histogram showing the collapses recorded by the accelerometric network and the permanent SNS array during the 14 collapse crises occurred in 2015

The time distribution of recorded collapses versus the daily total discharge measured at the Peschiera Springs (Fig. 4) highlights that the main collapse crises occur when a highest rate of discharge variation is observed, i.e. in correspondence with the yearly raising up and drowning down phases. During 2015, these phases, respectively, occurred in June–July 2015, when the SNS array recorded 482 collapses and the accelerometric network 118 ones, and in September 2015, when the SNS array recorded 168 collapses and the accelerometric network 26 ones. The SNS enlarged the sensibility field of the monitoring system down to 10^{-5} m s^{-2} for the PGA (average values between the two horizontal components) and to 10^{-11} m s^{-1} for the AI (average values between the two horizontal components) (Fig. 12). A more detailed analysis of the events occurred in correspondence with the main 2015 collapse crises (CC041 of May 31, CC046 of July 3, CC047 of July 15 and CC048 of July 25 reported in Table 1) was carried out. The collected data confirm that the accelerometric network is more reliable for detecting higher-energy events, whereas the SNS array shows a good response to detect also events characterized by low- to very low-energy (Fig. 13). Figure 8 shows the epicentral distribution of microseismic events. The events occurred during CC041 and CC046 collapse crises result located in the middle-eastern slope portion, near the C1 station of the accelerometric network. On the other hand, the microseismic events related to CC047 and CC048 collapse crises are located in the middle-southern portion of the slope; moreover, they are almost NNE-SSW aligned and follow the main scarps which bound and dislodge the portion of the slope involved in the rock mass spreading. The hypocentral location of the recorded events (Fig. 9) varies between 350 to 450 m a.s.l. and corresponds to a saturated rock mass volume where tensile stresses can be enucleated due to the interaction between effective stresses and ground water flow, according to Maffei et al. (2005) and Casini et al. (2006). The M_L value of the 2015 collapse crises ranges between −2.9 and −1.3.

Table 1 Data of the collapse crises occurred during 2015 which were measured by the accelerometric network and by the SNS array; data are not available (n.a.) when the SNS array was out-of-service

| Sequence of event ID	From date (dd/mm/yyyy)	To date (dd/mm/yyyy)	Accelerometric network (AN)					SNS array		Detection ratio (SNS/AN)
			Collapses (number)	Collapse frequency (number/h)	Max recorded intensity station	E_v max (m/s)	PGA_v max (m/s^2)	Collapses (number)	Collapse frequency (number/h)	
CC039	01-02-2015	01-02-2015	5	0.21	C6	4.77E−08	5.43E−03	11	0.46	2.2
CC040	09-05-2015	09-05-2015	8	0.33	C1	3.42E−07	1.46E−02	19	0.79	2.38
CC041	31-05-2015	31-05-2015	5	0.21	C1	5.61E−07	3.54E−03	23	0.96	4.6
CC042	06-06-2015	11-06-2015	42	0.29	C1	2.85E−05	1.68E−01	177	1.23	4.21
CC043	16-06-2015	17-06-2015	8	0.17	C1	1.24E−05	1.05E−01	19	0.4	2.38
CC044	20-06-2015	20-06-2015	3	0.13	C1	1.36E−07	1.15E−02	23	0.96	7.67
CC045	24-06-2015	24-06-2015	6	0.25	C1	1.52E−06	3.69E−02	n.a.	n.a.	n.a.
CC046	03-07-2015	03-07-2015	2	0.08	C1	1.50E−08	2.61E−03	59	2.46	29.5
CC047	15-07-2015	15-07-2015	8	0.33	C1	2.41E−07	1.30E−02	16	0.67	2
CC048	21-07-2015	25-07-2015	51	0.43	C1	9.71E−06	4.66E−02	247	2.06	4.84
CC049	07-08-2015	10-08-2015	38	0.4	C1	1.20E−06	3.55E−02	70	0.73	1.84
CC050	19-08-2015	19-08-2015	6	0.25	C1	1.82E−05	1.24E−01	n.a.	n.a.	n.a.
CC051	04-09-2015	05-09-2015	17	0.35	C1	3.84E−06	6.08E−02	149	3.1	8.76
CC052	13-09-2015	13-09-2015	5	0.21	C1	1.18E−04	3.22E−01	9	0.38	1.8
CC053	20-09-2015	20-09-2015	4	0.17	C1	1.03E−08	2.86E−03	10	0.42	2.5
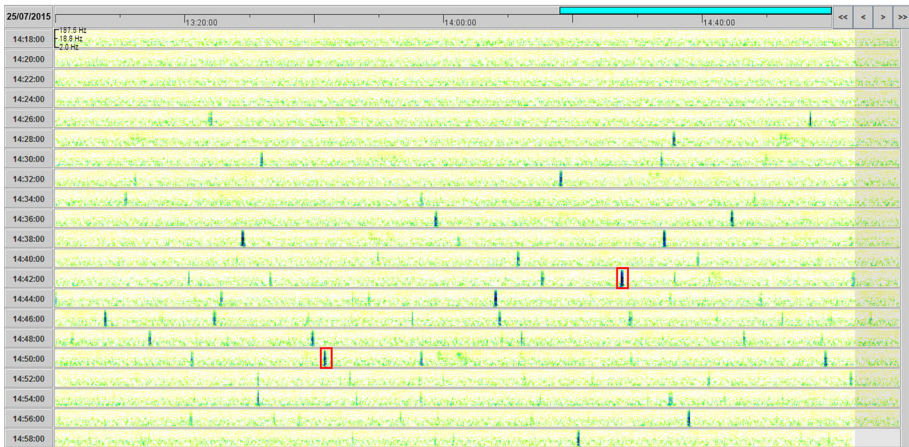
Fig. 11 Supersonogram from 14:18 to 15:00 UTC of 25 July 2015: 37 collapses are visible, the *red frames* indicate the 2 collapses recorded also by the accelerometric network
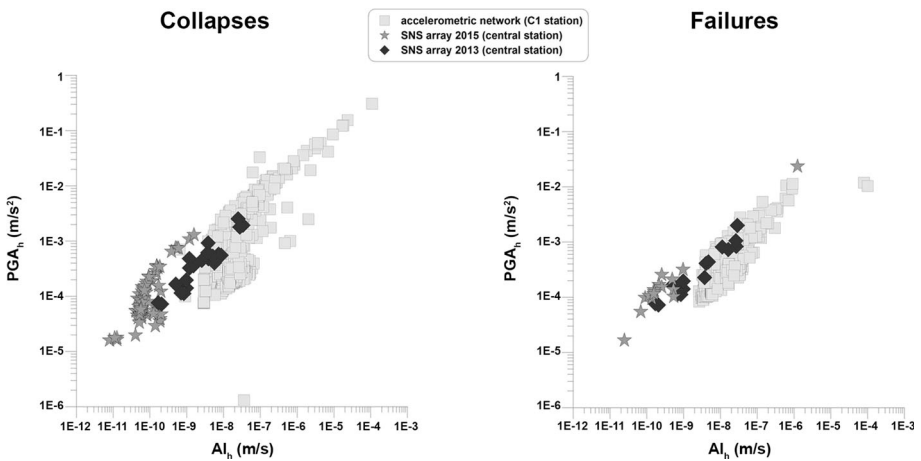

Fig. 12 PGA_h versus AI_h for the seismic events recorded by the accelerometric network, the 2013 temporary SNS array and the permanent SNS array

These results encourage to couple in future the nanoseismic data with the accelerometric ones for computing the control index $CI(P, t)$ and providing the related attention levels. Although evidences are not confirmed by each collapse crisis, in some cases it was observed a significant sequence of precursors that anticipates of some tens of minutes the strongest collapse (see the cases of CC041 and CC046 crises showed in Fig. 13). These outputs suggest that future records could provide better constrains to the evidences collected so far and allow to evaluate the possible role of precursors in early warning practice, i.e. by extending the "advice time" for the risk management.
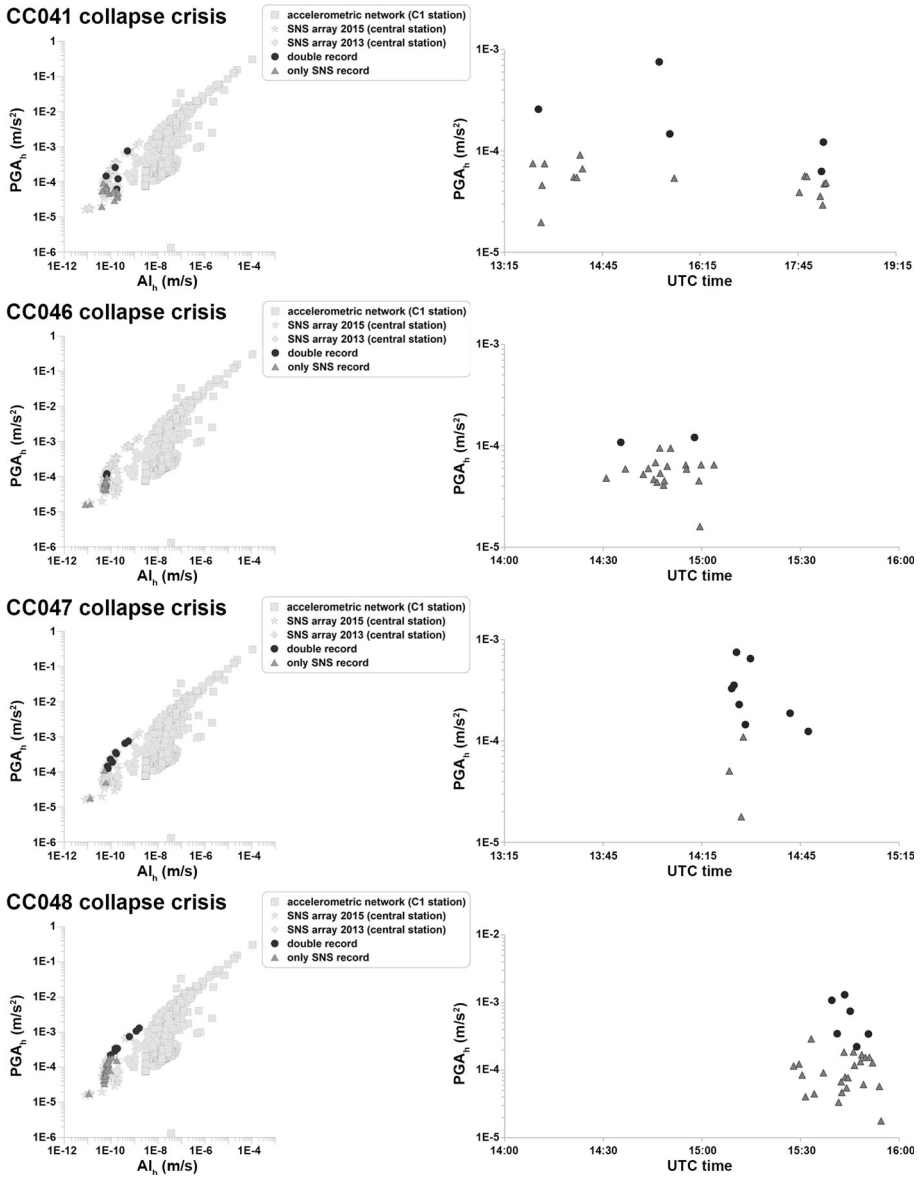
Fig. 13 PGA$_h$ versus AI$_h$ and PGA$_h$ versus time for the collapse events recorded during 4 collapse crises occurred on 2015

6 Summary and conclusions

The gravity-induced deformations involving the Peschiera Springs slope (Central Italy), hosting the main drainage plant of Rome aqueducts, are responsible for underground instabilities that involve the jointed rock mass. Since September 2008, an accelerometric network has been operating in the tunnels of the plant; during 7 years of monitoring, this

network recorded more than 2000 events, including earthquakes focused outside the slope as well as microseismic events (failures and collapses) originated within the slope and related to gravity-induced deformations.

In 2013, the accelerometric monitoring system was coupled with a temporary SNS nanoseismic array that was operative for 1 year and recorded 37 microseismic events related to underground instabilities. These events were distinguished in 19 collapses and 18 failures on the basis of the measured physical properties (i.e. time duration, frequency content, PGA and AI); the SNS array allowed also assessing hypocentres and M_L values of the detected events. Considering the hypocentre distribution, the recorded events result to be mostly concentrated in the eastern sector of the slope, in agreement with the intensely jointed conditions of the rock mass as well as the spatial distribution of the main landforms associated with the ongoing rock mass deformation. This result is also in good agreement with the tension–dissolution model of the Peschiera Springs slope, proposed in the literature by physical-analogue and numerical modelling to justify the ongoing gravity-induced deformations that involve the slope. More in particular, the failure events can be related to sliding along rock mass joints or to microcracking; on the other hand, collapses can be associated with underground instabilities of voids and caves that are induced by the intense dissolution processes and favoured by the high discharge of the karst aquifer.

The results obtained by the temporary SNS array led to the installation of a permanent SNS array in 2014. This array has been a useful tool for increasing the number of recorded microseismic events which mainly correspond to collapses, characterized by low- to very low-energy levels and by M_L ranging from −2.9 up to −1.3, as well as to locate them. The space distribution of the recorded collapses is remarkable in terms of correspondence with the surveyed landforms related to the ongoing deformational processes as well as with the saturated volume of the karts aquifer where tensile stresses can be enveloped within released rock mass bands. Moreover, the preliminary outputs in terms of time sequence of microseismic events obtained by the SNS permanent array encourage the prospect of future detection of precursors to enlarge the "advice time" in case of alert or emergency conditions so favouring the risk management of the monitored infrastructure.

References

Amitrano D, Arattano M, Chiarle M, Mortara G, Occhiena C, Pirulli M, Scavia C (2010) Microseismic activity analysis for the study of the rupture mechanism in unstable rock masses. Nat Hazard Earth Syst Sci 10:831–841

Bigi S, Costa Pisani P (2002) Structural setting of the Cicolano-M. Calvo area (Central Apennines, Italy). Boll Soc Geol Ital Spec 1:141–149

Boni CF, Bono P, Capelli G (1986) Schema idrogeologico dell'Italia Centrale. Mem Soc Geol Itali 35:991–1012

Boni CF, Capelli G, Petitta M (1995) Carta idrogeologica dell'alta e media Valle del F. Velino. Elaborazione cartografica e stampa System Cart, Roma

Butler R (2003) The Hawaii-2 observatory: observation of nanoearthquakes. Seismol Res Lett 74:290–297

Casini S, Martino S, Petitta M, Prestininzi A (2006) A physical analogue model to analyses interactions between tensile stresses and dissolution in carbonate slopes. Hydrogeol J 14:1387–1402

Ciotoli G, Di Filippo M, Nisio S, Romagnoli C (2001) La Piana di S. Vittorino: dati preliminari sugli studi geologici, strutturali, geomorfologici, geofisici e geochimici. Mem Soc Geol Itali 56:297–308

Deparis J, Jongmans J, Cotton F, Bailler L, Thouvenot F, Hantz D (2008) Analysis of rock-fall and rock-fall avalanche seismograms in the French Alps. Bull Seismol Soc Am 98(2):1781–1796

Evans S, Mugnozza GS, Strom A (2006) Landslides from massive rock slope failure. Nato Science Series. Springer, Netherlands. Series IV: Earth Environ Sci, vol 49, p 662

Fiorucci M, Iannucci R, Lenti L, Martino S, Paciello A, Prestininzi A, Rivellino S (2015) Seismic monitoring of the gravity-induced deformation involving the Peschiera Spring Slope (Italy) for the management of a main infrastructure. In: 6th international conference on earthquake geotechnical engineering, Christchurch, New Zealand, 1–4 November 2015, paper n 130

Got J-L, Mourot P, Grangeon J (2010) Pre-failure behaviour of an unstable limestone cliff from displacement and seismic data. Nat Hazard Earth Syst Sci 10:819–829

Hutchinson JN (1988) General report: morphological and geotechnical parameters of landslides in relation to geology and hydrogeology. In: Proceedings of 5th international symposium on landslides, Lausanne, Balkema, Rotterdam, pp 3–36

Joswig M (1990) Pattern recognition for earthquake detection. Bull Seismol Soc Am 80(1):170–186

Joswig M (1995) Automated classification of local earthquake data in the BUG small array. Geophys J Int 120:262–286

Joswig M (2008) Nanoseismic monitoring fills the gap between microseismic networks and passive seismic. First Break 26:121–128

Lenti L, Martino S, Paciello A, Prestininzi A, Rivellino S (2012) Microseismicity within a karstified rock mass due to cracks and collapses triggered by earthquakes and gravitational deformations. Nat Hazards 64:359–379

Lenti L, Martino S, Paciello A, Prestininzi A, Rivellino S (2015) Recorded displacements in a landslide slope due to regional and teleseismic earthquakes. Geophys J Int 201:1335–1345. doi:10.1093/gji/ggv063

Maffei A, Martino S, Prestininzi A (2005) From the geological to the numerical model in the analysis of the gravity-induced slope deformations: an example from the Central Apennines (Italy). Eng Geol 78:215–236

Martino S, Prestininzi A, Scarascia Mugnozza G (2004) Geological-evolutionary model of a gravity-induced slope deformation in the carbonate central Apennines (Italy). Q J Eng Geol Hydrogeol 37(1):31–47

Phillips WS, Pearson DC, Edwards CL, Stump BW (1997) Microseismicity induced by a controlled, mine collapse at white pine, Michigan. Int J Rock Mech Min Sci 34:314, paper 246

Savage WZ, Varnes DJ (1987) Mechanism of gravitational spreading of steep-sided ridges (''sackung''). Bull Int As Eng Geol 35:31–36

Sick B, Walter M, Joswig M (2014) Visual event screening of continuous seismic data by supersonograms. Pure appl Geophys 171(3):549–559. doi:10.1007/s00024-012-0618-x

Szwedzicki T (2003) Rock mass behaviour prior to failure. Int J Rock Mech Min Sci 40:573–584

Walter M, Schwaderer U, Joswig M (2012a) Seismic monitoring of precursory fracture signals from a destructive rockfall in the Vorarlberg Alps, Austria. Nat Hazards Earth Syst Sci 12:3545–3555

Walter M, Arnhardt C, Joswig M (2012b) Seismic monitoring of rockfalls, slide quakes and fissure development at the Super-Sauze mudslide, French Alps. Eng Geol 128:12–22

Wust-Bloch GH, Joswig M (2006) Pre-collapse identification of sinkholes in unconsolidated media at Dead Sea area by 'nanoseismic monitoring' (graphical jackknife location of weak sources by few, low-SNR records). Geophys J Int 167:1220–1232

Zischinsky U (1969) Uber Sackungen. Rock Mech 1:30–52